NANO LETTERS

LETTER

pubs.acs.org/NanoLett

Intrinsic Mechanisms of Memristive Switching

Kazuki Nagashima,[†] Takeshi Yanagida,[*,†,‡] Keisuke Oka,[†] Masaki Kanai,[†] Annop Klamchuen,[†] Jin-Soo Kim,[§] Bae Ho Park,[§] and Tomoji Kawai[*,†,§]

[†]Institute of Scientific and Industrial Research, Osaka University, 8-1 Mihogaoka, Ibaraki, Osaka 567-0047, Japan

[‡]PRESTO, Japan Science and Technology Agency, 4-1-8 Honcho, Kawaguchi, Saitama 332-0012, Japan

[§]Department of Physics, Division of Quantum Phases and Devices, Konkuk University, Seoul 143-701, Republic of Korea

S *Supporting Information*

ABSTRACT: Resistive switching (RS) memory effect in metal-oxide-metal junctions is a fascinating phenomenon toward next-generation universal nonvolatile memories. However the lack of understanding the electrical nature of RS has held back the applications. Here we demonstrate the electrical nature of bipolar RS in cobalt oxides, such as the conduction mechanism and the switching location, by utilizing a planar single oxide nanowire device. Experiments utilizing field effect devices and multiprobe measurements have shown that the nanoscale RS in cobalt oxides originates from redox events near the cathode with p-type conduction paths, which is in contrast with the prevailing oxygen vacancy based model.

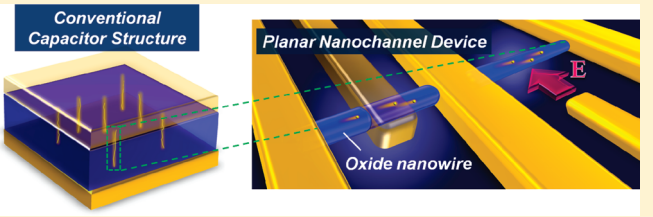

KEYWORDS: Resistive switching, nonvolatile memory, nanowires, p-type oxides, redox

Searching alternatives to current flash memory technology is one of the most crucial issues toward next generation high-density universal memories. Resistive switching (RS) in metal-oxide-metal (MOM) sandwich structures, frequently called as "ReRAM" and/or "Memristor", has the potential for such next-generation nonvolatile memories due to the structural simplicity and the memory characteristics superior to existing memories.[1−3] Numerous applications using Memristor have been proposed such as nonvolatile memory alternatives to flash memory, synaptic computing, reconfigurable logic circuit element and other circuit family.[4] However, the lack of knowledge as to the nature of RS has held back the practical RS memory applications. RS characteristics with different switching behaviors, including bipolar,[5−7] unipolar,[8−10] and threshold switching,[11,12] have been investigated in various oxides such as NiO,[9−15] TiO_2,[6−8,16−18] CuO,[19−21] CoO_x,[22−25] and others[26−30] with the intention being to explore the physical origins of RS and the exquisite materials for practical memory applications. A number of chemical and physical models[3,31,32] have been proposed to explain the RS events, and a filament model based on a rupture and formation of nanoscale conduction paths within insulators has most successfully explained many RS features.[1,3,5,6,8−12,14−30] Although investigations using a conductive atomic force microscopy (C-AFM),[15,18] a X-ray photoemission spectroscopy (XPS),[13,25] a Kelvin force microscopy (KFM),[24] a transmission electron microscopy (TEM),[8,22,33] and others[19−21,23,34] have been carried out to characterize such nanoscale conduction paths, the nanoscale physical and chemical origins of RS are still under debate due to the inherent difficulties in evaluating directly such internal nanoscale conduction paths within insulators. Some of these methods are unfortunately indirect and/or destructive, and more crucially identifying the exact location of such conduction paths is rather difficult since the conduction paths randomly distribute within the insulative layer. Utilizing lateral nanochannel structures might be one of promising ways to overcome the critical issue. The bottom-up approach using self-assembled oxide nanowires (∼10 nm scale size) offer the platform[35−40] to characterize directly and nondestructively the nanoscale conduction paths by confining the RS switching area and identifying the location of conduction paths. Previously, we have demonstrated the reliable bipolar RS[38] using a single MgO/cobalt oxide nanowire with 10^8 of the endurance; however the mechanisms of observed RS have not been identified. Compared with n-type oxides where oxygen vacancies play a crucial role on the RS events, understanding the RS conduction nature of p-type oxides such as cobalt oxides and nickel oxides, which exhibit the excellent memory characteristics,[9−15,19−25] is rather scarce due to the lack of direct experimental evidence to prove the RS conduction characteristics. In this letter, we demonstrate a nature of RS in p-type cobalt oxides, such as the conduction mechanism and the switching location, which cannot be clarified by conventional sandwich MOM structures, by utilizing a single cobalt oxide nanowire device.

Cobalt oxide nanowires composed of MgO core nanowire and cobalt oxide shell layer were fabricated by using an in situ nanowire template method (e.g., combination of vapor−liquid−solid (VLS) growth[41−43] and thin film growth), as reported elsewhere.[38−40,44−46] Cobalt oxide shell layer was deposited onto MgO nanowires[47−53] without atmospheric exposure to realize the well-defined heterointerfaces (the details of fabrication

Received: March 2, 2011
Revised: April 5, 2011
Published: April 08, 2011

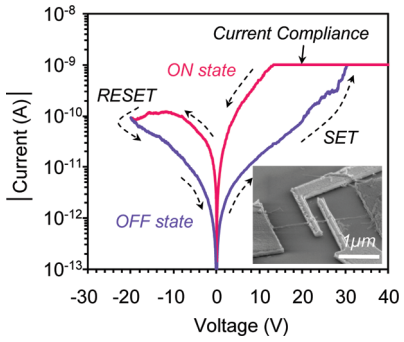

Figure 1. Typical $I-V$ characteristics of a Pt/cobalt oxide nanowire/Pt device. The compliance current was set to be 10^{-9} A. The inset shows the FESEM image of the nanowire device. The nanogap spacing in this device was ~250 nm.

process can be seen in Supporting Information). On the basis of the data of X-ray diffraction and optical absorption measurements, the cobalt oxide within nanowires was found to be a mixture of CoO and Co_3O_4, and CoO is rather dominant phase in the composite. The length and the diameter of MgO nanowires, and the thickness of cobalt oxide shell layer were typically 5 μm, 10 nm, and 5 nm, respectively. To construct single oxide nanowire devices, we utilized the following procedure. First, the cobalt oxide nanowires on the substrate were sonicated and dispersed into isopropanol, and then the nanowire suspension was transferred onto a phosphorus doped n-type silicon substrate capped with thermally oxidized SiO_2 layer with 300 nm of the thickness. Electron beam lithography was utilized to define nanoscale electrode patterns on the SiO_2/Si substrate, followed by metal deposition of Pt/Au (20 nm/100 nm).[54] The device structure was characterized by field emission scanning electron microscopy (FESEM) at 30 kV of an accelerating voltage. The transport measurements were performed at room temperature by using semiconductor parameter analyzer (Keithley 4200SCS) in various ambient atmosphere.

Figure 1 shows the typical current−voltage ($I-V$) data of a single cobalt oxide nanowire in a semilogarithmic current scale. The inset shows the FESEM image of the nanowire device employed. After the so-called forming process, which is defined as the initial process to introduce the electrical conduction within pristine insulative matrix by high electric field (~1.6×10^6 V/cm) (see Supporting Information), the devices exhibited the $I-V$ curves in Figure 1.[38] Hereafter the positively biased electrode during forming process is defined as "anode", while the grounded electrode is defined as "cathode". The polarity-dependent bipolar RS was consistently observed in all our devices with the compliance current of 10^{-9} A. When applying a positive electric field, a "SET" process from a high resistance OFF state (HRS) to a low resistance ON state (LRS) occurred, whereas a "RESET" process from LRS to HRS occurred when a negative electric field was applied. Note that the polarity of the electric field for the SET process was always consistent with the polarity of forming process. This indicates that the polarity of bipolar RS can be defined by the forming process since our Pt/nanowire/Pt structures are symmetric. In our single nanowire devices, the switching endurances were confirmed at least up to 10^8 times (see Supporting Information).[38] We utilize the stable nanowire RS devices to extract the nature of RS for cobalt oxides.

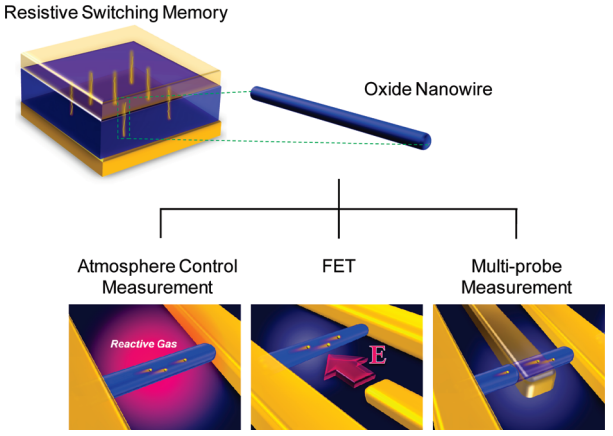

Figure 2. Schematic illustration of the strategy using a single oxide nanowire device.

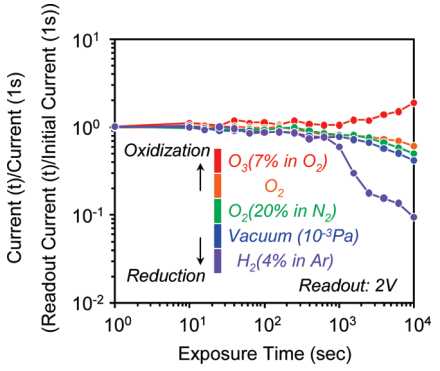

Figure 3. Retention data for the LRS conduction in the various reactive gases. The currents were read at 2 V.

Figure 2 shows our strategy by utilizing nanowire devices. As shown in Figure 2, we utilize the following three approaches: (i) atmosphere control measurement, (ii) planar field effect transistor (FET), and (iii) multiprobe measurement. For atmosphere control measurements, we intentionally utilize the chemical reactions with surroundings to extract the characteristics of conduction paths. Planar FET structures allow us to identify the carrier type of nanoscale conduction paths. Multiprobe measurement enables to identify the active switching location of RS. These approaches have been unfeasible in the thin film capacitor structures. By using these approaches, we will examine some previous implications as to RS mechanisms of cobalt oxides, including the RS conduction origin via oxygen vacancies or precipitation of metal components and the occurrence of RS near the anode.[23]

First, we examine the conducting characteristics of nanoscale RS by utilizing intentional chemical reactions with surroundings via introducing various reactive gases. Since a redox affects in principle the mobile carriers of oxides, the experiments allow us to identify and distinguish the conducting properties of RS. In RS, the LRS is a sort of electric-field-induced excited state and the HRS is the ground state (see Supporting Information), therefore the time evolution data of LRS during chemical reactions with surroundings should represent the nature of LRS conductions.[39] Figure 3 shows the retention data of the LRS current when varying the reactive atmosphere gases. The details of these

dx.doi.org/10.1021/nl200707n |Nano Lett. 2011, 11, 2114–2118

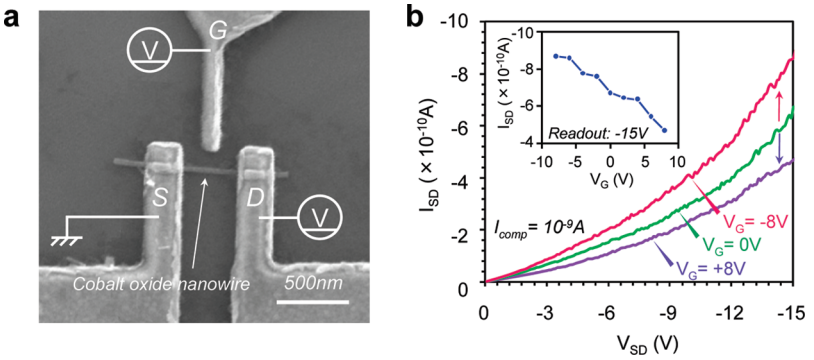

Figure 4. (a) FESEM image of the nanowire side gate FET structure. The nanogap spacing of $S-D$ (i.e., channel length) was ~400 nm. (b) $I_{SD}-V_{SD}$ characteristics of the cobalt oxide nanowire when varying the gate voltage (V_G) ranged from −8 to +8 V. Prior to applying the gate voltage, the device was switched into LRS and the stable $I_{SD}-V_{SD}$ curves in LRS were confirmed. (The distribution was within $\pm 0.3 \times 10^{-10}$A at −15 V) The compliance current was set to be 10^{-9} A. The inset shows the V_G dependence of I_{SD} measured at −15 V.

measurements can be seen in Supporting Information. The LRS current tended to decrease as the ambient gas was chemically reduced; see the data of H_2 contained gas. On the contrary, the LRS current tended to increase for an oxidizing atmosphere, for example, O_3-contained gas. These results indicate two important factors on the nanoscale RS mechanisms of cobalt oxides. First, the redox events must be closely related to the occurrence of bipolar RS in cobalt oxides since the LRS conduction is strongly dependent on the occurrence of redox in atmospheres. Second, the trend of chemical reactions with surroundings on LRS conductions seems to be consistent with p-type oxide semiconductors, because in the case of p-type oxides hole carriers must be compensated by a reduction or enhanced by an oxidization. Such p-type nature of conducting characteristics in RS of cobalt oxides is in fact inconsistent with previous implications, where frequently the oxygen vacancies or the precipitations of Co metals were assumed to be an origin of conduction paths within insulative cobalt oxide matrix.[22] If the presence of oxygen vacancies or Co metals is responsible for the RS conduction, the LRS conductivity must decrease with an oxidation, which is completely opposite to the present experimental trend. Even considering the possibility of the coexistence of Co metal and p-type conduction paths, the decrease of LRS current when reducing the atmosphere cannot be explained because the LRS current must be maintained in the presence of Co metal conduction paths. These experimental results highlight that redox events with p-type conduction paths play a crucial role on a bipolar nanoscale RS of cobalt oxides.

The carrier type of LRS conduction can be directly identified by utilizing the nanowire FET structure. Figure 4a shows the FESEM image of the planar FET structure composed of source (S), drain (D), and gate (G) electrodes. In the FET experiments, a negative voltage was applied to the drain and the source was grounded. The details of the SET process can be seen in Supporting Information. In the devices, the operation current and the electric field intensity levels for the SET and RESET processes were comparable with the data of Figures 1. After performing the SET process, the electric field was applied between the gate and the source electrodes. Figure 4b shows $I_{SD}-V_{SD}$ curves of the cobalt oxide nanowires when varying the gate voltages (V_G), where I_{SD} and V_{SD} are the current and voltage between drain and source, respectively. Note that the range of all I_{GS} with varying V_G was at least 2 orders of magnitude smaller than that of I_{SD}, indicating negligible effects of current leakage in these measurements. I_{SD} decreased when applying the positive +8 V of V_G, whereas I_{SD} increased for the negative −8 V of V_G. The inset of Figure 4b shows V_G dependence of I_{SD} measured at −15 V. I_{SD} systematically decreased with increasing V_G. These results clearly confirmed that the major carriers of the LRS conduction are holes (i.e., p-type). It should be noted that all obtained implications are not consistent with the prevailing "anodic oxidization" model for cobalt oxides.

Here we describe a model for bipolar RS in cobalt oxides based on above experimental trends. During the forming process, negatively charged oxygen ions move toward the anode under the high electric field, resulting in an excess oxygen phase (i.e., cation vacancies)[55−58] near the anode. The continuous migration of oxygen ions results in the paths of cation vacancies from the anode to the cathode. In fact, this presenting model is an inverse analogue of an anodic oxidization model for n-type oxides in which the local conduction paths are comprised of oxygen vacancies.[5,59] Since a conductivity of bulk cobalt oxides is well-known to originate in cation vacancies (i.e., $Co_{1-\delta}O$ and/or $Co_{3-\delta}O_4$),[55−58] cation vacancies induced by ion migrations result in the p-type conduction paths from the anode to the cathode. Although oxygen vacancies should be also created near the cathode, their contributions on the electrical conductivity must be low since the formation energy of oxygen vacancies in cobalt oxides is much higher than that of cation vacancies, and the donor level is far from the conduction band.[60,61] After the forming process completes, the junction resistance switches into LRS, and the hole carriers flow through the p-type conduction paths composed of cation vacancies. When the electric field with the opposite polarity is applied, the depletion of cation vacancies occurs from the cathode via the migration of oxygen vacancies, resulting in the disconnection of conduction path (RESET process) near the cathode. SET process can occur by applying a voltage with the opposite polarity via accompanying the reconnection of cation vacancies. Note that these our implications completely differ from prevailing model based on an anodic oxidization for RS of cobalt oxides.[23] This presenting model based on p-type conduction with cation vacancies strongly infers that RS must occur near the cathode. Therefore, we examine the active switching location of RS by utilizing multiprobe measurements. Figure 5a shows the FESEM image of the nanowire device employed for multiprobe measurements. Three electrodes were chosen and defined as "electrode A", "electrode B", and "electrode C". First, we performed the forming process between the

dx.doi.org/10.1021/nl200707n |*Nano Lett.* 2011, 11, 2114–2118

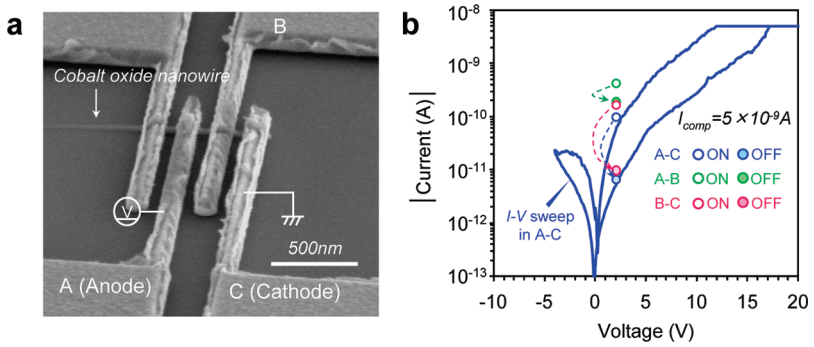

Figure 5. (a) FESEM image of a single cobalt oxide nanowire device bridged between multielectrodes. The nanogap spacing in this device was ~100 nm. Three electrodes were chosen and named as electrode A, electrode B, and electrode C. The voltage was applied to the electrode A, while the electrode C was grounded for RS operations. (b) Typical $I-V$ characteristics obtained in the multiprobe nanowire devices. The compliance current was set to be 5×10^{-9} A. The opened and the filled circles respectively show the LRS and HRS currents measured in each configurations (A-C (blue), A-B (green), and B,C (pink)).

Table 1. A Series of Resistance Data Obtained in the Multiprobe Measurements

measured area	ON state resistance (Ω)	OFF state resistance (Ω)	ON/OFF ratio
A(anode)-C(cathode)	2.06×10^{10}	3.02×10^{11}	14.7
A-B(anode side)	4.74×10^{9}	1.06×10^{10}	2.2
B-C(cathode side)	1.20×10^{10}	2.05×10^{11}	17.1

electrode A and the electrode C (A-C) by applying relatively high electric fields. We applied the positive voltage to the electrode A (i.e., anode) and the electrode C was grounded (i.e., cathode) during the forming process. After the forming process, the device exhibited the reliable bipolar RS behavior with the current compliance of 5×10^{-9} A as shown in Figure 5b. In order to identify the active switching location of the bipolar RS between A-C electrodes, we utilized the electrode B to measure the resistances changes in A-B (anode side) and B-C (cathode side) during RS. Table 1 and Figure 5b show the resistance variations of A-B and B-C in both LRS and HRS. In LRS, which is induced by SET process, the resistance values of A-B (anode side) and B-C (cathode side) were 4.74×10^{9} and 1.20×10^{10} Ω, respectively. Although this result indicates that the anode side is slightly conductive, the difference was not so significant. On the other hand, in the HRS induced by RESET process, the resistance values of A-B and B-C were 1.06×10^{10} and 2.05×10^{11} Ω, respectively. Obviously, the resistance of B-C near the cathode is one order magnitude higher than that of A-B near the anode. Note that this trend was confirmed in all samples measured. These results indicate that the bipolar RS in cobalt oxides occurs near the cathode rather than the anode, since the resistance of anode side was not significantly modified by RESET process. Although this implication contradicts previous reports,[23] where they insisted that the anode interface is responsible for bipolar RS of cobalt oxides, this might be due to the device structures since they used the Ta layer at the anode interface in which the Ta layer (possibly Ta-oxides) rather than cobalt oxides might be responsible. Thus these results successfully demonstrated the active switching location for the bipolar RS of cobalt oxides with the direct experimental evidence and also were in good agreement with the presenting model based on p-type conduction paths comprised of cation vacancies. The suggested model seems to be able to capture the many features of bipolar RS not only for cobalt oxides but also for more generally p-type oxides.

In conclusion, we have investigated the nature of RS in cobalt oxides by using a single cobalt oxide nanowire. Our results have demonstrated that the nanoscale RS of cobalt oxides originates from redox events within p-type conduction paths. This implication completely differs from the prevailing anodic oxidization model based on oxygen vacancies. Multiprobe measurements using the nanowire RS devices have successfully identified that the nanoscale RS of cobalt oxides mainly occurs near the cathode in good agreement with our model based on p-type conduction. Since the properties of RS electrical conductions, which we have revealed herein, must be well understood for designing RS devices, the present findings as to the carrier transports and the nanoscale redox reactions on RS of cobalt oxides will provide a foundation not only to understand the complex nature of RS in metal-oxide-metal junctions with the microscopic view but also for tailoring the RS properties in high density nanoscale nonvolatile memory device applications.

■ ASSOCIATED CONTENT

Supporting Information. Further experimental details, structural analysis, electrical measurements, data retention measurement in air, and atmosphere dependent forming process. This material is available free of charge via the Internet at http://pubs.acs.org.

■ AUTHOR INFORMATION

Corresponding Author

*E-mail: (T.Y.) yanagi32@sanken.osaka-u.ac.jp; (T.K.) kawai@sanken.osaka-u.ac.jp. Tel.: +81-6-6879-4294. FAX: +81-6-6879-4295.

■ ACKNOWLEDGMENT

This work was supported in part by SCOPE and NEXT Project. T.K. and B.H.P. were partly supported by WCU program through the NRF funded by the MEST (Grant R31-2008-000-10057-0). T.K. was supported by FIRST program.

REFERENCES

(1) Waser, R.; Aono, M. *Nat. Mater.* **2007**, *6*, 833–839.
(2) Strukov, D. B.; Snider, G. S.; Stewart, D. R.; Williams, R. S. *Nature* **2008**, *453*, 80–83.
(3) Waser, R.; Dittmann, R.; Staikov, G.; Szot, K. *Adv. Mater.* **2009**, *21*, 2632–2663.
(4) Pershin, Y. V.; Di Ventra, M. *Adv. Phys.* **2011**, *60*, 145–227.
(5) Szot, K.; Speier, W.; Bihlmayer, G.; Waser, R. *Nat. Mater.* **2006**, *5*, 312–320.
(6) Yang, J. J.; Pickett, M. D.; Li, X.; Ohlberg, D. A. A.; Stewart, D. R.; Williams, R. S. *Nat. Nanotechnol.* **2008**, *3*, 429–433.
(7) Yang, J. J.; Borghetti, J.; Murphy, D.; Stewart, D. R.; Williams, R. S. *Adv. Mater.* **2009**, *21*, 3754–3758.
(8) Kwon, D.-H.; Kim, K. M.; Jang, J. H.; Jeon, J. M.; Lee, M. H.; Kim, G. H.; Li, X.-S.; Park, G.-S.; Lee, B.; Han, S.; Kim, M.; Hwang, C. S. *Nat. Nanotechnol.* **2010**, *5*, 148–153.
(9) Lee, M.-J.; Han, S.; Jeon, S. H.; Park, B. H.; Kang, B. S.; Ahn, S.-E.; Kim, K. H.; Lee, C. B.; Kim, C. J.; Yoo, I.-K.; Seo, D. H.; Li, X.-S.; Park, J.-B.; Lee, J.-H.; Park, Y. *Nano Lett.* **2009**, *9*, 1476–1481.
(10) Ahn, S.-E.; Lee, M.-J.; Park, Y.; Kang, B. S.; Lee, C. B.; Kim, K. H.; Seo, S.; Suh, D.-S.; Kim, D.-C.; Hur, J.; Xianyu, W.; Stefanovich, G.; Yin, H.; Yoo, I.-K.; Lee, J.-H.; Park, J.-B.; Baek, I.-G.; Park, B. H. *Adv. Mater.* **2008**, *20*, 924–928.
(11) Chang, S. H.; Lee, J. S.; Chae, S. C.; Lee, S. B.; Liu, C.; Kahng, B.; Kim, D.-W.; Noh, T. W. *Phys. Rev. Lett.* **2009**, *102*, 026801.
(12) Chang, S. H.; Chae, S. C.; Lee, S. B.; Liu, C.; Noh, T. W.; Lee, J. S.; Kahng, B.; Jang, J. H.; Kim, M. Y.; Kim, D.-W.; Jung, C. U. *Appl. Phys. Lett.* **2008**, *92*, 183507.
(13) Martinez, E.; Guedj, C.; Calka, P.; Minoret, S.; Buckley, J.; Bernard, Y.; Jousseaume, V. *Surf. Interface Anal.* **2010**, *42*, 783–786.
(14) Kawai, M.; Ito, K.; Ichikawa, N.; Shimakawa, Y. *Appl. Phys. Lett.* **2010**, *96*, 072106.
(15) Son, J. Y.; Shin, Y.-H. *Appl. Phys. Lett.* **2008**, *92*, 222106.
(16) Nauenheim, C.; Kuegeler, C.; Ruediger, A.; Waser, R. *Appl. Phys. Lett.* **2010**, *96*, 122902.
(17) Song, S. J.; Kim, K. M.; Kim, G. H.; Lee, M. H.; Seok, J. Y.; Jung, R.; Hwang, C. S. *Appl. Phys. Lett.* **2010**, *96*, 112904.
(18) Shin, Y. C.; Lee, M. H.; Kim, K. M.; Kim, G. H.; Song, S. J.; Seok, J. Y.; Hwang, C. S. *Phys. Status Solidi RRL* **2010**, *4*, 112–114.
(19) Fujiwara, K.; Yajima, T.; Nakamura, Y.; Rozenberg, M. J.; Takagi, H. *Appl. Phys. Exp.* **2009**, *2*, 081401.
(20) Yasuhara, R.; Fujiwara, K.; Horiba, K.; Kumigashira, H.; Kotsugi, M.; Oshima, M.; Takagi, H. *Appl. Phys. Lett.* **2009**, *95*, 012110.
(21) Fujiwara, K.; Nemoto, T.; Rozenberg, M. J.; Nakamura, Y.; Takagi, H. *Jpn. J. Appl. Phys.* **2008**, *8*, 6266–6271.
(22) Shima, H.; Nakano, T.; Akinaga, H. *Appl. Phys. Lett.* **2010**, *96* 192107.
(23) Shima, H.; Takano, F.; Muramatsu, H.; Akinaga, H.; Tamai, Y.; Inque, I. H.; Takagi, H. *Appl. Phys. Lett.* **2008**, *93*, 113504.
(24) Shima, H.; Takano, F.; Muramatsu, H.; Yamazaki, M.; Akinaga, H.; Kogure, A. *Phys. Status Solidi RRL* **2008**, *2*, 99–101.
(25) Shima, H.; Takano, F.; Tamai, Y.; Akinaga, H.; Inoue, I. H. *Jpn. J. Appl. Phys.* **2007**, *46*, L57–L60.
(26) Kinoshita, K.; Okutani, T.; Tanaka, H.; Hinoki, T.; Yazawa, K.; Ohmi, K.; Kishida, S. *Appl. Phys. Lett.* **2010**, *96*, 143505.
(27) Zhang, H.; Gao, B.; Sun, B.; Chen, G.; Zeng, L.; Liu, L.; Liu, X.; Lu, J.; Han, R.; Kang, J.; Yu, B. *Appl. Phys. Lett.* **2010**, *96*, 123502.
(28) Goux, L.; Chen, Y.-Y.; Pantisano, L.; Wang, X.-P.; Groeseneken, G.; Jurczak, M.; Wouters, D. J. *Electrochem. Solid-State Lett.* **2010**, *13*, G54–G56.
(29) Nagashima, K.; Yanagida, T.; Oka, K.; Kawai, T. *Appl. Phys. Lett.* **2009**, *94*, 242902.
(30) Chen, M.-C.; Chang, T.-C.; Huang, S.-Y.; Chen, S.-C.; Hu, C.-W.; Tsai, C.-T.; Sze, S. M. *Electrochem. Solid-State Lett.* **2010**, *13*, H191–193.
(31) Sawa, A. *Mater. Today* **2008**, *11*, 28–36.
(32) Hickmott, T. W. *J. Appl. Phys.* **1962**, *33*, 2669–2682.
(33) Park, G.-S.; Li, X.-S.; Kim, D.-C.; Jung, R.-J.; Lee, M.-J.; Seo, S. *Appl. Phys. Lett.* **2007**, *91*, 222103.
(34) Yajima, T.; Fujiwara, K.; Nakao, A.; Kobayashi, T.; Tanaka, T.; Sunouchi, K.; Suzuki, Y.; Takeda, M.; Kojima, K.; Nakamura, Y.; Taniguchi, K.; Takagi, H. *Jpn. J. Appl. Phys.* **2010**, *49*, 060215.
(35) Chang, W.-Y.; Lin, C.-A.; He, J.-H.; Wu, T.-B. *Appl. Phys. Lett.* **2010**, *96*, 242109.
(36) Herderick, E. D.; Reddy, K. M.; Sample, R. N.; Draskovic, T. I.; Padture, N. P. *Appl. Phys. Lett.* **2009**, *95*, 203505.
(37) Kim, S. I.; Lee, J. H.; Chang, Y. W.; Hwang, S. S.; Yoo, K.-H. *Appl. Phys. Lett.* **2008**, *93*, 033503.
(38) Nagashima, K.; Yanagida, T.; Oka, K.; Taniguchi, M.; Kawai, T.; Kim, J.-S.; Park, B.-H. *Nano Lett.* **2010**, *10*, 1359–1363.
(39) Oka, K.; Yanagida, T.; Nagashima, K.; Kawai, T.; Kim, J.-S.; Park, B. H. *J. Am. Chem. Soc.* **2010**, *132*, 6634–6635.
(40) Oka, K.; Yanagida, T.; Nagashima, K.; Tanaka, H.; Kawai, T. *J. Am. Chem. Soc.* **2009**, *131*, 3434–3435.
(41) Klamchuen, A.; Yanagida, T.; Nagashima, K.; Seki, S.; Oka, K.; Taniguchi, M.; Kawai, T. *Appl. Phys. Lett.* **2009**, *95*, 053105.
(42) Klamchuen, A.; Yanagida, T.; Kanai, M.; Nagashima, K.; Oka, K.; Kawai, T.; Suzuki, M.; Hidaka, Y.; Kai, S. *Appl. Phys. Lett.* **2010**, *97*, 073114.
(43) Klamchuen, A.; Yanagida, T.; Kanai, M.; Nagashima, K.; Oka, K.; Seki, S.; Suzuki, M.; Hidaka, Y.; Kai, S.; Kawai, T. *Appl. Phys. Lett.* **2011**, *98*, 053107.
(44) Nagashima, K.; Yanagida, T.; Tanaka, H.; Seki, S.; Saeki, A.; Tagawa, S.; Kawai, T. *J. Am. Chem. Soc.* **2008**, *130*, 5378–5382.
(45) Marcu, A.; Yanagida, T.; Nagashima, K.; Oka, K.; Tanaka, H.; Kawai, T. *Appl. Phys. Lett.* **2008**, *92*, 173119.
(46) Oka, K.; Yanagida, T.; Nagashima, K.; Tanaka, H.; Seki, S.; Honsho, Y.; Ishimaru, M.; Hirata, A.; Kawai, T. *Appl. Phys. Lett.* **2009**, *95*, 133110.
(47) Yanagida, T.; Marcu, A.; Matsui, H.; Nagashima, K.; Oka, K.; Yokota, K.; Taniguchi, M.; Kawai, T. *J. Phys. Chem. C* **2008**, *112*, 18923–18926.
(48) Nagashima, K.; Yanagida, T.; Oka, K.; Tanaka, H.; Kawai, T. *Appl. Phys. Lett.* **2008**, *93*, 153103.
(49) Yanagida, T.; Nagashima, K.; Tanaka, H.; Kawai, T. *J. Appl. Phys.* **2008**, *104*, 016101.
(50) Yanagida, T.; Nagashima, K.; Tanaka, H.; Kawai, T. *Appl. Phys. Lett.* **2007**, *91*, 061502.
(51) Marcu, A.; Yanagida, T.; Nagashima, K.; Tanaka, H.; Kawai, T. *J. Appl. Phys.* **2007**, *102*, 016102.
(52) Nagashima, K.; Yanagida, T.; Tanaka, H.; Kawai, T. *J. Appl. Phys.* **2007**, *101*, 124304.
(53) Nagashima, K.; Yanagida, T.; Tanaka, H.; Kawai, T. *Appl. Phys. Lett.* **2007**, *90*, 233103.
(54) Nagashima, K.; Yanagida, T.; Klamchuen, A.; Kanai, M.; Oka, K.; Seki, S.; Kawai, T. *Appl. Phys. Lett.* **2010**, *96*, 073110.
(55) Wdowik, U. D.; Parlinski, K. *Phys. Rev. B* **2008**, *77*, 115110.
(56) Hed, A. Z. *J. Chem. Phys.* **1969**, *50*, 2935–2937.
(57) Shinde, V. R.; Mahadik, S. B.; Gujar, T. P.; Lokhande, C. D. *Appl. Surf. Sci.* **2006**, *252*, 7487–7492.
(58) Kadam, L. D.; Patil, P. S. *Mater. Chem. Phys.* **2001**, *68*, 225–232.
(59) Jeong, D. S.; Schroeder, H.; Breuer, U.; Waser, R. *J. Appl. Phys.* **2008**, *104*, 123716.
(60) Tarento, R. J.; Harding, J. H. *J. Phys. C: Solid State Phys.* **1987**, *20*, L677–L680.
(61) Tarento, R. J. *Rev. Phys. Appl.* **1989**, *24*, 643–647.